Laboratory Plate Loading Test on Calcareous Sands from a Hydraulic fill Reef Island

Xing Wang
Guangzhou University
YANG WU (308622435@qq.com)
Guangzhou University
Jie Cui
Guangzhou University
Chang-qi Zhu
Wuhan Institute of Rock and Soil Mechanics Chinese Academy of Sciences
Xin-zhi Wang
Wuhan Institute of Rock and Soil Mechanics Chinese Academy of Sciences

Research Article

Keywords: Reef island, Plate loading tests, Bearing capacity, Deformation modulus, Stress dispersion angle

Posted Date: April 20th, 2021

DOI: https://doi.org/10.21203/rs.3.rs-336245/v1

Abstract

The landforms and vertical strata distribution characteristics of Yongxing Island show that the reclaimed reef island is characterized by soft upper strata (calcareous sand) and hard lower strata (reef limestone). In this study, a series of plate loading tests was conducted to examine the influences of particle gradation, compactness, and moisture condition on the bearing mechanism and deformation properties of the calcareous sand foundation. When the foundation is shallowly buried, the relative density range corresponding to a calcareous sand foundation exhibiting local shear failure is narrower than that of a terrigenous sand foundation. For the same compactness, dry calcareous medium sand has a much larger bearing capacity and deformation modulus than dry calcareous fine sand. The effect of water on the bearing capacity of the calcareous medium sand is greater than the effect on calcareous fine sand. Its weak cementation and low permeability make the initial deformation of saturated calcareous fine sand slightly smaller than that under dry conditions. The stress dispersion angle of the calcareous medium sand foundation is 52°, which is larger than that of terrigenous sand. A larger stress dispersion angle leads to a higher bearing capacity and deformation modulus than those of terrigenous sand.

Highlights

- The geological characteristics of sample location site was summarized.
- Laboratory plate loading test results on calcareous sand foundation were presented.
- Particle gradation, compactness, and moisture condition greatly affected the bearing mechanism and deformation properties of calcareous sand foundation.
- The failure mode of calcareous sand foundation was identified and analyzed.
- The lateral stress distribution and stress dispersion angle of calcareous sand foundation were measured.

1. Introduction

Calcareous sand, also known as coral sand or carbonate sand, is mainly composed of calcium carbonate and magnesium carbonate. Its geological formation involves physical, biochemical, and chemical processes following the death of marine organisms such as reef coral, shells, and algae. Calcareous sand is commonly found on continental shelves and coastlines between 30ºN and 30ºS (Fig. 1), such as in the South China Sea (Wang et al. 2017a), the Persian Gulf (McClelland 1988), the Northwest Continental Shelf of Australia (King and Lodge 1988), the Campus and Sergipe basins in southern Brazil (Mello et al. 1989), the Red Sea in the Middle East (Hagenaar 1982; Hakami and Abu Seif 2019), the Gulf of Mexico in Central America, and the Caribbean Sea (Dutt and Ingram 1988). Calcareous sand is also distributed in the Bass Strait (Wiltise et al. 1988).

Due to the characteristics of its distribution, calcareous sand is widely used in marine engineering as backfill materials for hydraulic reclamation of reef islands, road embankments, and airport runways.

Because of its special marine biogenesis, calcareous sand has obvious regional characteristics, and its engineering characteristics are also quite different from those of terrigenous quartz sand (Ohno et al. 1999). Insufficient understanding of the engineering characteristics of calcareous sand has caused serious geo-hazards.

In the early 1960s, calcareous sand and reef limestone were discovered in the first borehole core samples collected during offshore geological exploration in the Persian Gulf. The engineers reported that the borehole core sample contained a large quantity of shell fragments, and that the calcium carbonate content was high, but little attention was paid to its engineering characteristics (Liu et al. 1995; Alba and Audibert 1999). The lack of knowledge and understanding of the mechanical behavior of calcareous sand is the main reason why it has not been given adequate attention by engineers (McClelland 1988).

In 1968, as driven piles were being installed for an Iranian Lavan offshore oil platform, a pile about 1.0 m in diameter fell freely under its own weight after passing through an 8.0-m-thick, well-cemented, calcareous sand layer in the seabed. The pile stopped sinking when it penetrated a reef limestone layer at a depth of about 23.0 m, which provided sufficient bearing capacity. Because the underground water level at the construction site was shallow, and the pile uplift resistance requirement for the structure was low, the problem of calcareous sand causing the pile to fall freely had not been given sufficient attention (Alba and Audibert 1999; Wang et al. 2011).

In the early 1970s, a project in the Bass Strait, Australia attracted scholars' attention to the foundation design and construction on a calcareous sand layer for the first time. In 1970, when ESSO Petroleum Co. Ltd. constructed the first offshore oil platform in the Bass Strait, they found that the piles easily penetrated into the calcareous sand layer. Considering the bearing capacity of the pile after installation, the engineers carried out uplift loading testing on a 0.67 m pile section, and they found that its actual bearing capacity was only 20% of its designed value. In order to remedy this deficiency, the engineers revised the pile foundation construction design. The driven piles were eventually replaced by bored piles at a high cost (Alba and Audibert 1999) Subsequently, engineers became very conservative when dealing with calcareous sand layers, and bored piles were frequently used for the construction of offshore structures (Wess and Chamberlin 1971). In addition, as ocean exploration entered further and deeper sea areas where the terrigenous sediments nearly disappeared, the traditional design method was not applicable for construction of offshore oil and gas platforms in the deep sea (Angemeer et al. 1973). The engineers were motivated to thoroughly investigate the engineering characteristics of calcareous sand.

In addition, the North Rankin "A" platform is located on the northwestern continental shelf of Australia; it is currently the largest structure built on a marine calcareous sand layer. The design plan required that a pile with a diameter of 1.83 m be completely embedded within the calcareous sand layer in order for it to provide sufficient bearing capacity. In the early stage of construction, the engineers repeatedly demonstrated the feasibility of the design based on on-site geological survey data and laboratory model tests. However, the pile detection results showed that the pile did not meet the design requirements, and

the subsequent reinforcement measures were very expensive (King and Lodge 1988). Since this project, scholars have treated calcareous sand as a special soil.

At present, many researchers have carried out several studies on the engineering properties of calcareous sand and have obtained fruitful results (Shaqour 2007; Lee et al. 2012; Gai et al. 2013; Lv et al. 2017; Liu et al. 2018; Shen et al. 2018;Ye et al. 2019; Rui et al. 2020; Liu et al. 2020). However, most of these research results are limited to the study the engineering characteristics of calcareous sand supporting a pile foundation (Lin et al. 2016; Hazzar et al. 2017; Ma et al. 2018; Page et al. 2018; Lee et al. 2019; Sui et al. 2019), while research on shallow foundations on calcareous sand are limited (Wang et al. 2011; Barari and Ibsen 2017). Calcareous sand is the only material used for island reclamation in the South China Sea. Moreover, the height of the buildings on reef islands is generally low, so shallow foundations are widely used in reef island infrastructure construction. Due to the lack of relevant design parameters for the bearing capacity and deformation characteristics of calcareous sand foundations, engineers typically construct a shallow foundation on calcareous sand by referencing the design scheme and parameters of a shallow foundation on terrigenous quartz sand. However, the engineering characteristics of calcareous sand are significantly different from those of terrigenous quartz sand. The blind application of seemingly relevant design parameters of a shallow foundation on terrigenous quartz sand could lead to design defects and engineering disasters.

This study presents the results of a series of plate loading tests conducted on calcareous sand layers retrieved from Yongxing Island in the Xisha Islands under various test conditions. The geologic characteristics of the sample location site where a hydraulic reclamation project is ongoing in the South China Sea are summarized. The influences of particle gradation, compactness, and moisture condition on the bearing mechanism and deformation properties of calcareous sand layers are examined through plate loading tests. The differences between the engineering characteristics of a calcareous sand foundation and an ordinary terrigenous quartz sand foundation are identified from the perspective of the stress dispersion angle. The failure mode of a calcareous sand layer is analyzed and compared to that of terrigenous quartz sand. The results of this study further our understanding of the engineering characteristics of calcareous deposits in hydraulic reclamation construction sites.

2. Site Geology

The Xisha Islands, also known as the Paracel Islands, are the central part of the area bounded by the Chinese mainland, the Dongsha Islands, the Hainan Islands, the Zhongsha Islands, and the Nansha Islands. They are composed of the Yongle and Xuande atolls, which are the largest islands in the South China Sea. Yongxing Island (16°49'53"N, 112°20'22"E), a typical lime-sand island, is the largest of the Xisha Islands in terms of land area (Fig. 2a). Yongxing Island is about 800 m from nearby Rocky Island. They were originally two separate islands, but due to the construction of the airport runway on Yongxing Island and the increase in the number of hydraulic reclamation projects, the two islands have been connected to form a new island (Fig. 2b). The expanded Yongxing Island has an irregular shape. Its long

axis (3191 m) trends nearly east-west, whereas its short axis (1576 m) trends northwest-southeast. The total area of the island is about 3.01 km^2, and the terrain is flat (Wang et al. 2018).

2.1. Landforms

Yongxing Island is located on the southwest side of Xuande Atoll. Yongxing Island is a butterfly shaped depression with a low middle and high sides, with heights of up to 5–8 m. The different sedimentary dynamic conditions of the middle and sides of the island have resulted in the overall annular distribution of Yongxing Island's geomorphology. From offshore to the center of the island, the landforms are as follows: reef front slope, reef flat, beach, sand dike, sand mat, and marsh land (Fig. 3).

The reef front slope lies below the low tide surface where many live corals grow, with scattered shell fragments and coral branches on the gentle slope. There is a breaker zone between the reef front slope and the reef flat. The broken waves carry 0.2–0.3 m coral reef blocks and biological sand grains to this area from the reef front slope, forming a bank-like reef ridge. The reef ridge is 0.2–0.5 m higher than the low tide surface, and it is about 100 m wide.

The height of the reef flat is usually the same as that of the low tide surface. It is a basic component of the reef and determines the size and shape of the reef. The width of the reef flat around Yongxing Island varies significantly, but is generally 400–800 m. The widest part (i.e., the northeastern part of the reef) reaches 1500 m. The sediments within the reef flat are mainly composed of the remains of shallow-water stony corals, shells, algae, and forams. The particle size of the sediments, especially that of the gravel, decreases from the leading edge of the reef flat to the beach, and some sand debris can be found near the beach. Most of these sediments originate from the reef front slope and are brought to the reef flat by broken waves. Some debris from reef flat organisms can also be found. During low tide, 0.05–0.50 m of sea water remains in most areas on the reef flat, and scattered gullies, ponds, and clusters of living corals are exposed on the reef flat.

The beach is a special landform formed by waves moving sand debris from the reef flat to the intertidal zone. The slope angles of the leading and trailing edges of Yongxing Island's beach are 3–9°, and the width of the beach is about 20–40 m. Due to the surge effect, the height difference of the beach berm can reach 1 m, with a width of 2–6 m and a reverse slope angle of about 1.2° (Yu et al. 1995). The beach sediments are mainly calcareous medium sand. Some of the cemented rocks in the northwestern part of the reef are exposed and inclined towards the sea, with an inclination of about 6°. Due to the southwestern monsoon climate, in the summer, the beach on the southwestern part of the island is heavily eroded by broken waves, and the beach surface becomes narrower. After the construction on Yongxing Island, the concrete road between Yongxing Island and Rocky Island and the beach between the airport runways on the eastern and southern reef flats form the shape of an unsealed sack (Fig. 2). This area contains a large amount of coral fragments, which can be used as fill material for construction projects.

The sand debris blown up onto the beach by the sea wind have migrated and piled up above the high tide level, forming sand dikes. The height of the sand dikes determines the elevation of the reef island, i.e., they are the highest points on the island. Yongxing Island has several sand dikes connected to each other in the approximate form of a closed circle. The sand dike extending from the northwestern side of the reef island to the northeastern side is 100–150 m wide, 6–8 m high, and the slope angle of the sand dike on the northwestern side of the island is about 32°. The dike extending from the eastern side to the southern side has a gentle slope, a width of 80–100 m, and a height of 4–6 m. The sediments that make up the sand dike are mainly calcareous medium-coarse sand. Calcareous sand debris, the remains of forams and mollusks are the major component of these sediments.

The sand mat is located in the transition zone between the back edge of the sand dike and the marsh land. The sand mat is a special landform generated by the sea wind driving coral fragments over the top of the sand dike, resulting in the deposition of coral fragments from the leeward slope of the sand dike to the edge of the marsh land. The slope of the sand mat is very shallow. The sand mats on Yongxing Island are the main landform units, and the main area in which the reef island vegetation grows. The height of the sand mats is generally greater than 2.0 m, and the width of the sand mats can be up to 500.0 m. The sand mat is mainly composed of calcareous medium-coarse sand, and the biological composition of the sediment is similar to that of the sand dike. However, the sand mat contains a small amount of quartz sand, which is actually spilled terrigenous sand debris, which was used in the construction of reef islands in recent years (Yu et al. 1995).

A shallow reef pond was formed by the water surrounding the sand dike. As the sand mat expanded, the reef pond gradually dried up and shrunk, resulting in the formation of marsh land containing stagnant water. The water content of the sediments in the marsh land is high, and some plants live in this area. Because the marsh land is far from the reef flat and the wind has a limited carrying ability, the sediment in the marsh land is mainly composed of calcareous medium-fine sand. The alternating monsoon climate of the sea leads to the alternate deposition of poorly sorted calcareous sand debris in the marsh land. Mollusk shells, calcium algae, and coral fragments are the main components of the sediment in marsh land, and the foram content is also high.

In summary, the sediments in the different geomorphological areas of Yongxing Island have significantly different particle sizes and biological compositions. The calcareous biodebris in the reef flat and the reef front slope is the source of the sediments on Yongxing Island. Due to the short migration distance of the calcareous sediments and the retention of some of the characteristics of the protozoa, the sediments have a highly irregular particle shape, are generally coarse, and the particle size gradually decreases from offshore to the inland area. The horizontal distribution characteristics of the sedimentary strata of Yongxing Island also indicate that except for the reef front slope, all of the geomorphologic areas can be used as building sites. This conclusion is confirmed by the distribution of the existing buildings on Yongxing Island.

2.2. Stratum structure

In order to investigate the distribution characteristics of the longitudinal stratigraphic structure of Yongxing Island, a series of geological drilling tests was carried out on Yongxing Island and neighboring Rocky Island in the 1970s and 1980s. The results revealed that Yongxing Island is a lime-sand island that accumulated on the annular reef flat of the present coral atolls, and the accumulated materials are reef debris, biogenetic sand, and gravel. The development of Yongxing Island is closely related to the neotectonic movements, monsoon waves, sea level changes, the development of the reef flat, and the changes in the atoll lagoon (Lv et al. 1987). Based on analysis of borehole core samples obtained from wells Xiyong 1, Xiyong 2, and Xishi 1, a schematic diagram of the Yongxing Island-Rocky Island stratigraphic section was constructed (Fig. 4) (Zhang 1990). Fig. 4 shows that a coral reef packstone framework underlies the weakly cemented, coral fragment deposits at approximately 30.00 m (Well XY 1), 17.72 m (Well XY 2), and 24.68 m (Well XS 1). That is, Yongxing Island and Rocky Island are both binary geologic structures with soft upper strata and hard lower strata developed on a reef flat (Zhang 1990; Wang et al. 2018).

3. Material And Methods

3.1. Test material

The test material was calcareous sand collected from Yongxing Island in the South China Sea, specifically from the shallow marsh land at the center of Yongxing Island (Fig. 2). In order to investigate the effect of the particle size distribution on the calcareous sand layer's response under plate loading conditions, two types of calcareous sand with different particle gradations were collected from different positions within the same geomorphic area of the island. Before the test, the particle size distribution curve was determined according to the relevant specifications of the Chinese National Standard of Soil Test Methods (GB/T50123–2019). According to Fig. 5, the two types of calcareous sand used in the tests are classified as fine and medium sand. The gradation curve of the calcareous fine sand is steep, and the particle size distribution range is relatively concentrated. The mass of the 0.10–0.25 mm particles accounts for 57.3% of the total sample mass, making it calcareous fine sand with poor gradation. The particle size distribution range of the calcareous medium sand is large, but the smoothness of its gradation curve is poor; thus, it is also categorized as a calcareous sand with poor gradation.

Table 1

Physical parameters of two types of calcareous sands with different particle gradations.

Sample	d_{10} (mm)	d_{30} (mm)	d_{50} (mm)	d_{60} (mm)	C_u	C_c	Specific gravity G_s	Minimum dry density ρ_{dmin} (g/cm^3)	Maximum dry density ρ_{dmax} (g/cm^3)
Calcareous fine sand	0.11	0.16	0.21	0.24	2.18	0.97	2.78	1.21	1.56
Calcareous medium sand	0.07	0.19	0.39	0.58	8.29	0.89	2.78	1.30	1.84

Before the test, the physical parameters of both types of sand were tested according to the relevant provisions of the Chinese National Standard of Soil Test Methods (GB/T50123–2019). Table 1 shows that the specific gravities of the two calcareous sands are identical. The maximum and minimum dry densities of the calcareous fine sand are less than those of the calcareous medium sand, which is attributed to the difference in the gradation parameters of the two types of sand.

3.2. Experiment scheme

The purpose of this paper is to symmetrically examine the influences of particle gradation, compactness, and moisture condition on the bearing capacity and deformation characteristics of calcareous sand foundations. Based on our field investigation of the hydraulic reclamation calcareous sand foundation on Yongxing Island in the South China Sea, the relative density of the calcareous sand in the foundation treated by vibroflotation is more than 69%. It is believed that the calcareous sand foundation is constructed in a dense state. Under the action of hydraulic seepage, the untreated foundation soil also reaches a medium-dense state. Therefore, the relative densities of the calcareous sands are set as 69% (dense), 55% (medium- -dense), and 42% (medium-dense) to evaluate the influence of the compactness on the load-deformation results acquired from the plate loading tests. The water content range of the calcareous sand foundations on the reef island is large, and it becomes particularly large over the tidal cycle. In this study, the tests were conducted on a calcareous sand layer under dry and saturated conditions. In addition, in order to eliminate the influence of the size of the loading plate on the test results, the distance between the boundary of the loading plate and the edge of the model box was about three times the width of the loading plate. Because the dimension of the model box used in the test was 900 mm × 900 mm (length × width), a square loading plate with a side length of 130 mm was used to carry out the laboratory plate loading tests. The specific testing conditions are shown in Table 2.

Table 2

Laboratory plate loading test scheme.

Test No.	Sample	Dimensions of loading plate (length × width × thickness) (mm)	Moisture condition	Relative density *Dr*
1	Calcareous fine sand	130×130×20	Dry	69%
2	Calcareous fine sand	130×130×20	Dry	55%
3	Calcareous fine sand	130×130×20	Dry	42%
4	Calcareous fine sand	130×130×20	Saturated	69%
5	Calcareous medium sand	130×130×20	Dry	69%
6	Calcareous medium sand	130×130×20	Dry	55%
7	Calcareous medium sand	130×130×20	Dry	42%
8	Calcareous medium sand	130×130×20	Saturated	69%

3.3.Test equipment

As shown in Fig. 6, the model test device used for the plate loading tests was composed of a model box, a reaction frame, a loading plate, a static loading system, and a lateral stress measurement system.

The model box was made by welding together 10 mm thick steel plates. The overall shape of the box is square, with an inner dimension of 900 mm × 900 mm × 1000 mm (length × width × height). The reaction frame consisted of three parts: a bottom beam, a side column, and a top beam. The model box was placed on two concrete piers, which were the same height as the bottom beam of the reaction frame, and the spacing was slightly larger than the width of the bottom beam. The bottom beam of the reaction frame passed through the bottom of the model box and was placed symmetrically corresponding to the model box. In order to enhance the integrity of the test device, the bottom beam of the reaction frame was welded to the area in contact with the bottom of the model box. The side column of the reaction frame was connected to the bottom beam and the top beam using nuts, and multiple thread sets were continuously arranged at the top of the side column, so that the top beam could be moved vertically by adjusting the position of the nuts according to the filling height of the sample in the model box, forming a movable reaction frame with a variable top beam height. The bottom beam and the top beam were made of I-shaped steel with a high rigidity.

3.3.1. Static loading system

The static loading system mainly included three parts: a jack, an oil pump and oil tube, and a static loading tester. The static loading tester was composed of an oil pressure sensor, a displacement sensor, a data control box, and a data acquisition system, as shown in Fig. 7.

3.3.2. Lateral stress measurement system

The lateral stress measurement system consisted of three parts, as shown in Fig. 8: a soil pressure gauge, a data collector, and a microcomputer processing system.

To obtain the lateral stress distribution of the calcareous sand foundation during loading and to calculate the stress dispersion angle, the soil pressure gauge measured the lateral stress at different depths. The soil pressure gauge used in this test was a KDC–200kPa vibrating wire soil pressure gauge produced by the Tokyo Institute of Instruments, Japan (Fig. 8a). The high accuracy soil pressure gauge was less affected by temperature and water. It had a shell diameter of 100 mm, a sensing area diameter of 92 mm, and a thickness of 20.5 mm. Its measuring range is 0–200 kPa with an accuracy of 0.1 kPa, which is well within the accuracy requirements of this test. The data device was a CR1000 data collector manufactured by Campbell Company, United States (Fig. 8b). This data collector is equipped with many data transmission interfaces, and the signal is stable and reliable.

3.4. Test method

The entire testing process was divided into three stages: preparation, sample filling, and loading. The detailed steps are as follows.

(1) The sample was spread out and dried in an exposed place. Its water content was measured before filling, and the mass of each sand layer was pre-calculated for each layer according to the designated compactness level.

(2) Several lines were drawn at intervals of 100 mm along the depth direction around the inner wall of the model box with white paint (Fig. 9), in order to keep the position constant and for ease of identification during the filling process.

(3) Nine soil pressure gauges connected with a data collector were fixed to the inner wall of the model box from bottom to top, ensuring one gauge per each 100 mm within the sand layer (Fig. 9). Prior to loading, a microcomputer processing system was used to set the initial gauge reading to zero.

(4) The samples were added in a total of 9 layers, each with a thickness of 100 mm. A platform scale with a precision of 10 g was used to weigh the sand used in each filling to ensure that the mass of each 100 mm layer was consistent with the test design and that the sample density was uniform.

(5) A tape measure was used to locate the center position of the sample's surface in the model box, and the loading plate was placed at the center position on the sample's surface, which was leveled with a leveling rod.

(6) After the components of the static loading system were assembled in sequence, the jack connected to the oil tube was placed at the center position on the loading plate, and the oil pump was used to lift the jack rod until it reached the bottom of the reaction frame's top beam.

(7) The beam supported on the side wall of the model box was positioned so that it was perpendicular to the reaction frame on both sides of the loading plate (Fig. 6). The displacement sensors were affixed to both beams using magnetic bases, and their initial values were set to zero.

(8) After all the preparation work was completed, the soil sample was allowed to stand for 24 hours. The loading began after the loading plate was settled and stabilized under the weight of the jack. Note that when a saturated sample was tested, after all of the preparation work was completed, water was continuously injected into the model box until the sample surface was just barely submerged, and the loading was carried out after the soil sample was allowed to stand for 24 h.

The results of previous studies show that the settlement of a calcareous sand foundation under loading can be stabilized within two hours (Wang et al. 2017b). Therefore, the rapid loading method can be used to implement the plate loading tests. The stabilization time of each loading stage was set as two hours following methods of previous investigations. The magnitude of the load in each stage was selected according to the compactness of the sample and the estimated amount of settlement under the loading. The test continued until shear failure occurred or until the sample's deformation reached the limit specified in the Chinese National Code for the Design of Building Foundations (GB50007–2019), i.e., 25 mm. In addition, to make the loading results comparable under different testing conditions, the characteristic value of the bearing capacity of all of the plate loading tests were determined using the following criteria. (1) When the P-S curve had a significant proportional load limit, the proportional load limit was taken as the characteristic value of the bearing capacity. (2) When the proportional load limit of the P-S curve was more than half the ultimate bearing capacity, half of the ultimate bearing capacity was defined as the characteristic value. It is worth noting that according to the relevant provisions of the Chinese National Code for the Design of Building Foundations (GB50007–2019), the maximum settlement of shallow foundations should not exceed 25 mm. Therefore, when the settlement of the loading plate reached 25 mm, but there was no visible sign of failure, the load stress at approximately 25 mm was taken as the ultimate bearing capacity of the calcareous sand foundation. (3) When the significant proportional load limit could not be determined from the P-S curve, the load corresponding to $S/B = 0.010–0.015$ was selected as the characteristic value of the bearing capacity. In addition, the deformation modulus E_0 reflects the stiffness of the foundation under loading. Thus, in this study, we used the deformation modulus E_0 to analyze the deformation characteristics of the calcareous sand foundation under the above described test conditions. The deformation modulus E_0 can be calculated as follows:

$$E_0 = I_u(1-\mu^2)\frac{Pd}{S} \quad (1)$$

where I_u is the settlement influence coefficient associated with the shape of the loading plate, and 0.88 is used for a square loading plate. μ is the Poisson's ratio of the foundation soil. In this study, μ = 0.25 is assumed. d is the characteristic dimension of the square loading plate, i.e., its side length. P is the proportional limit load of the foundation soil corresponding to the base stress at the end of the linear section of the P-S curve of the plate loading test. If there is no visible linear section in the P-S curve, the corresponding load at S/B = 0.010–0.015 is used. S is the settlement of the foundation soil corresponding to load P.

4. Test Results, Discussion, And Analysis

4.1. Influence of compactness

In this study, dry calcareous fine sands with relative densities of 69%, 55%, and 42% were used to investigate the influence of compactness on the bearing capacity and deformation characteristics of calcareous sand foundations. The test results are shown in Fig. 10.

Fig. 10 shows the following: (1) as the relative density increases, the bearing capacity and the deformation modulus of the calcareous fine sand foundation significantly increase. In engineering applications, the bearing capacity increment and the settlement could be reduced by increasing the density of the foundation. (2) The calcareous sand foundations with various relative densities exhibited different failure modes. The failure mode of a compacted calcareous sand foundation with a relative density of 69% is general shear failure, whereas a medium-dense calcareous sand foundation with a relative density of 55% is characterized by local shear failure, and its P-S curve has no visible inflection point. The calcareous sand foundation with a relative density of 42% is near the boundary between the medium-dense state and the low-dense state, and although it falls within the medium-dense category characterized by a relative density Dr, its P-S curve exhibits a punching shear failure mode, which differs from the failure mode on a terrigenous quartz sand foundation with the same relative density. Vesic used a quartz sand foundation to systematically investigate the influence of the compactness and burial depth of a foundation on the failure mode of the foundation soil (Vesic 1973). It was found that when the burial depth of the foundation is zero, the relative density boundary corresponding to the different failure modes of the foundations is approximately consistent with the sand compactness demarcation characterized by the relative density Dr. That is, a dense quartz sand foundation (Dr=66.7–100%) corresponds to general shear failure, a medium-dense quartz sand foundation (Dr=33.3–66.6%) corresponds to local shear failure, and a low-dense quartz sand foundation (Dr=0.0–33.2%) corresponds to punching shear failure. According to the test results in this study, when the burial depth of the foundation is zero, the failure modes of calcareous sand foundations are mainly general shear failure and punching shear failure, and

the compactness range characterized by the relative density corresponding to local shear failure is narrow. The special failure mode of a calcareous sand foundation under shallow foundation loading can be attributed to its extremely irregular particle shape and fragile nature under low stresses. The medium-dense calcareous sand foundation and the medium-dense quartz sand foundation have the same relative densities, but the shape of the calcareous sand particles is highly irregular, so the calcareous sand foundation has a larger void ratio than the quartz sand foundation (Wang et al. 2019). Particle breakage also results in the deformation of the calcareous sand foundation being greater than that of the quartz sand foundation under the same conditions (Wang et al. 2019), making it more likely that punching shear failure will occur in a calcareous sand foundation, increasing the compactness range characterized by the relative density corresponding to punching shear failure, and decreasing the compactness range characterized by the relative density corresponding to local shear failure.

4.2. Effects of gradation

Gradation is an important parameter for characterizing the physical properties of sand, and relevant studies have shown that gradation has significant effects on the mechanical properties of calcareous sand (Wang et al. 2017c; Lu et al. 2018; Lv et al. 2019). In order to evaluate the effects of gradation on the engineering characteristics of calcareous sand foundations, plate loading tests were conducted on calcareous fine sand and calcareous medium sand at relative densities of 69%, 55%, and 42% under dry condition. The results are shown in Fig. 11.

Fig. 11 shows that the bearing capacity and deformation characteristics of calcareous sand foundations are influenced by gradation. For the same compactness and moisture condition, the bearing capacity and deformation modulus of a calcareous medium sand foundation are higher than that of a calcareous fine sand foundation. There are two reasons for this. (1) As shown in Table 1, although both sands are calcareous sands with poor gradation, the gradation of the calcareous medium sand is better than that of the calcareous fine sand. There is no marked difference in the curvature coefficients C_c of the two sands, but there is a significant difference in their uniformity coefficients C_u. The uniformity coefficient C_u of the calcareous fine sand is 2.18 (C_u<5), and the particle size is uniform, mostly within 0.10–0.25 mm. Under the same conditions, the uniformity coefficient C_u of the calcareous medium sand is 8.29 (C_u>5), its particle size distribution is wide, its gradation is better, and its shear strength resistance and stiffness are higher. (2) The two types of sand were collected from adjacent areas on the same reef island and have the same specific gravity G_s, so the influence of mineral composition on the test results can be neglected. The maximum and minimum dry densities of the calcareous medium sand are both greater (and its void ratio is less) than those of the calcareous fine sand, and the distribution range of the dry density (and void ratio) of the calcareous medium sand is also wider. Thus, the two calcareous sands with different particle gradations have the same relative density D_r, but their dry densities (and void ratios) are quite different. Taking calcareous medium sand and calcareous fine sand with a relative density of D_r=69% as examples, for two sands with the same relative density, the dry density ρ_d of the calcareous medium sand

can reach 1.63 g/cm^3 (void ratio e=0.71), while the dry density ρ_d of the calcareous fine sand is only 1.43g/cm^3 (void ratio e=0.94). The dry density ρ_d of the calcareous medium sand is larger (and its void ratio e is smaller) than that of the calcareous fine sand, so the bearing capacity and deformation modulus of a calcareous medium sand foundation are larger.

4.3. Effects of moisture condition

To examine the influence of the moisture condition on the bearing capacity and deformation modulus of a calcareous sand layer, a 130 mm × 130 mm (length × width) rectangular loading plate was used to simulate a shallow foundation in this study. The differences in the bearing capacities and deformation characteristics of the calcareous fine sand foundation and the calcareous medium sand foundation with a relative density of 69% were studied under both dry and saturated conditions. The results are shown in Fig. 12.

Fig. 12 shows that (1) the bearing capacity of the calcareous fine sand foundation with a relative density of 69% under saturated conditions is about 61.5% of that under dry conditions. When the load on the saturated calcareous fine sand is increased from 0 to 400 kPa, the foundation remains stable. When loaded to 450 kPa, the settlement of the loading plate suddenly increases. The settlement amount at 450 kPa is about 3.8 times that at 400 kPa. It is impossible to attain 500 kPa of loading. Before the point of instability was reached, the loading plate was immersed in the soil, and the surrounding soil was uplifted and cracked. The failure mode exhibited the characteristics of local shear failure, and the total settlement was 15.09 mm. The dry calcareous fine sand foundation shows signs of instability when loaded to 550 kPa, and it reached its maximum bearing capacity at 650 kPa, with a total settlement of 26.98 mm. (2) The initial deformation of the dry calcareous medium sand foundation was small, and the settlement developed steadily under loading throughout the entire process. At the maximum output stress of the jack (1200 kPa), the foundation failure was still not visibly noticeable, and the final settlement was only 18.25 mm. The initial deformation of the saturated calcareous medium sand foundation was large, and the bearing capacity of the saturated foundation was low. The cumulative settlement of the foundation was 15.2 mm when it was loaded to 500 kPa. At 500 kPa, the settlement of the foundation during the current loading process was 2.3 times that of the previous loading, and the total settlement was 19.1 mm. Therefore, for the same relative density, the bearing capacity of the dry calcareous medium sand foundation was more than twice that under saturated conditions. (3) The deformation modulus of the dry calcareous medium sand foundation (17.52 MPa) was higher than that (2.84 MPa) in the saturated state. However, the deformation modulus of the dry calcareous fine sand foundation (6.15 MPa) was lower than that (10.57 MPa) in the saturated state. The deformation modulus refers to the stress level required to attain a unit settlement considering the combined effects of the loading plate's shape and size and the actual soil stress state. The difference between the deformation modulus of the calcareous fine sand foundation and the calcareous medium sand foundation is due to the difference in the interaction mechanism of the water surrounding the calcareous sand particles.

The calcareous fine sand grains are finer, and when completely saturated, the water tightly bonds the loose calcareous fine sand grains together to form a weakly-cemented medium with a certain strength and rigidity (Fig. 13b). In the early stage of the loading test, the shear force that destroys the foundation soil not only resists the shear resistance caused by the sliding of the particles, it also destroys the force caused by the cementation of the particles. Therefore, when the dry and saturated foundation soils reach the same settlement level, the load on the saturated soil is higher than that on the dry soil. As the foundation settlement increases with increasing applied stress, the particle cementation is weakened. At this time, the relative movement of the particles is lubricated by the water, which greatly weakens the bearing capacity of the foundation soil. The P-S curve of the saturated soil is characterized by a sharp increase in the settlement of the loading plate as the loading increases (Fig. 12a). In contrast, since the calcareous medium sand is coarser and there is no firm cementation between the particles when saturated (Fig. 13), the increase in the water content only serves to reduce the shear resistance as the particles move relative to each other. In the beginning of the test, when unit settlement occurs, the load applied to the saturated calcareous medium sand foundation is smaller than that applied under dry conditions. Secondly, because the particle size of the calcareous fine sand is smaller than that of the calcareous medium sand, the dissipation rate of the pore water stress of the saturated calcareous fine sand is slower than that of the saturated calcareous medium sand. This is another reason why the bearing capacity of the saturated calcareous fine sand foundation is larger than that of the saturated calcareous medium sand foundation in the early stage of the test.

5. Stress Dispersion Angle

When a normal load is applied to the loading plate, the lower part of the foundation soil will undergo shear failure within a certain range. Thus, the stress dispersion angle (θ) is usually used to measure the range of the failure of the foundation soil subjected to an external force. The stress dispersion angle is the angle between the stress dispersion boundary line and the vertical direction in the foundation soil (Fig. 14). Previous studies have been conducted to examine the range of the stress dispersion of foundation soils under loading (Liu et al. 2007; Zhang et al. 2010; Chung et al. 2011; Wang et al. 2016). However, these studies mostly focused on composite foundations, and the foundation material used was terrigenous soil. Few studies have been conducted on the stress dispersion pattern of calcareous sand foundations under loading, so whether the stress dispersion angle range of a calcareous sand foundation is consistent with the results of previous studies remains to be determined. The data from the soil pressure gauges show that the variation pattern of the lateral stress with loading and depth is identical under different test conditions (compactness, gradation, and moisture condition), but the magnitudes of the recorded values are different. The variation in the lateral stress on a calcareous sand foundation with load and depth is discussed by taking the dry calcareous medium sand with a relative density of 69% as an example. The stress dispersion angle of a calcareous sand foundation under a static load was calculated using the measured data. In order to avoid reinforcement effects after the soil pressure gauges are embedded in the foundation soil and to facilitate their embedding, the soil pressure gauges were numbered and pasted on the side wall of the model box, as shown in Fig. 14.

Fig. 15 shows the variation in the lateral stress at different depths (#1–#9) in the foundation soil, illustrating the following points. (1) Except for individual discrete points, the lateral stress at different depths in the foundation soil increases as the base stress increases. This is because the increase in the base stress causes the vertical stress in the foundation soil to increase, and the lateral stress also increases with increasing base stress when the change in the soil's coefficient of lateral pressure at rest is not large. (2) The lateral stress at different depths in the foundation soil increases as the base stress increases. During the entire loading process, the lateral stress at gauge #4 increases from 2.49 kPa to 11.36 kPa, i.e., by about 356%. The increase in the lateral stress was the smallest at gauge #1, only 33.8%. This result is due to the range of the stress dispersion in the foundation soil during the loading. Gauge #1 and the loading plate are at the same horizontal level, and the stress dispersed at gauge #1 during the loading process is very small. The increase in the lateral stress at gauge 1# is mainly caused by compression of the lateral foundation soil during the forced sinking of the loading plate. Due to the small lateral compression force, the total increase in the lateral stress at gauge #1 is only 2.46 kPa. Gauge #4 is near the boundary line of the internal stress dispersion of the foundation soil, and although the foundation soil at depths greater than that of gauge #4 is in the foundation soil stress dispersion range, the base stress gradually decreases with increasing depth, so the lateral stress is the largest at gauge #4. (3) The lateral stress is relatively small at all depths within the foundation soil, which is related to the data acquisition configuration and the stress mode of the foundation soil. The soil pressure gauges were set to 0 before the loading began, so the readings only reflect the increase in the lateral stress due to net base pressure. Secondly, due to the large size of the soil pressure gauge, the soil pressure gauge was pasted on the internal surface of the model box. The horizontal distance of the gauges from the loading plate was about three times the width of the loading plate. This results in the readings measured by the soil pressure gauge being smaller, but it does not affect the regularity of the test results.

Fig. 16 shows the variation in the lateral stress inside the foundation soil with increasing depth under different additional base stress levels. Fig. 16 illustrates the following. (1) The lateral stress in the foundation soil initially increases and then decreases with increasing depth under different base stress levels. The maximum lateral stress occurs at about 300 mm below the bottom of the foundation, corresponding to soil pressure gauge #4, which is reinforced by the conclusion drawn from Fig. 15. Accordingly, the stress dispersion angle in the calcareous medium sand foundation is about 52º, which is larger than the 30º stress dispersion angle for an ordinary terrigenous sand foundation reported in the *Chinese National Code for the Design of Building Foundations* (GB50007–2019). Thus, the range of stress dispersion in a calcareous sand foundation is wider than that in an ordinary terrigenous sand foundation. This finding also confirms the conclusion that from the perspective of the stress dispersion angle, the bearing capacity of a calcareous sand foundation is greater than that of a quartz sand foundation under the same conditions (Wang et al. 2011). (2) At depths of greater than 600 mm, the lateral stress in the foundation soil increases again, and this increase becomes more pronounced with increasing depth. The boundary effect of the bottom plate of the model box is the main cause of this phenomenon. Under loading, the vertical deformation of the foundation soil at the bottom of the model

box is limited, and it can only be displaced to both sides to reduce the increasing vertical stress, which increases the lateral stress on the soil. The closer the position is to the bottom plate of the model box, the greater the lateral stress becomes.

6. Conclusions

The following conclusions are drawn based on the results of this study.

1) The bearing capacity and deformation modulus of a calcareous sand foundation increases with increasing compactness. When a calcareous sand foundation is not embedded deeply, its main failure modes are general shear failure and punching shear failure. The density range of sand characterized by relative density corresponding to the local shear failure of a calcareous foundation in narrow compared with that of terrigenous quartz sand.

2) The bearing capacity and deformation characteristics of calcareous sand foundations are significantly influenced by gradation. For the same compactness, the bearing capacity and deformation modulus of a dry calcareous medium sand foundation are generally larger than those of a dry calcareous fine sand foundation.

3) The influence of moisture condition on the bearing capacity of a calcareous medium sand foundation is larger than that on a calcareous fine sand foundation. For the same compactness, the bearing capacity of saturated calcareous medium sand is less than 50% of that under dry conditions, and the bearing capacity of saturated calcareous fine sand is about 61.5% of that under dry conditions.

4) Weak cementation and low permeability make the initial rigidity of saturated calcareous fine sand slightly larger than that under dry conditions, but the initial rigidity of calcareous medium sand under saturated condition is much smaller than that under dry condition.

5) The stress dispersion angle of a calcareous medium sand foundation is about 52º, which is larger than that of an ordinary terrigenous sand foundation. This is also the main reason why the bearing capacity and deformation modulus of a calcareous sand foundation are both larger than those of an ordinary terrigenous quartz sand foundation.

Declarations

Acknowledgments

This research was funded by the China Postdoctoral Science Foundation (Nos. 2020M682653), the Guangdong Basic and Applied Basic Research Foundation (Nos. 2020A1515110663), the National Natural Science Foundation of China (Nos. 41877271, 51908153), the Strategic Priority Research Program of the Chinese Academy of Sciences (XDA13010301), and the Guangzhou City Technology and Science Program (201904010278).

References

1. Alba JL, Audibert JME (1999) Pile design in calcareous and carbonaceous granular materials, an historic overview. In: Proceedings of the Second International Conference on Engineering for Calcareous Sediments, Manama, Bahrain, Vol. 1, Rotterdam, A.A. Balkema, pp. 29–44.
2. Angemeer J, Carlson E, Klick JH (1973) Techniques and results of offshore pile load testing in the calcareous soils. In: Proceedings of the 5th Annual Offshore Technology Conference, Houston, American.
3. Barari A, Ibsen LB (2017) Insight into the lateral response of offshore shallow foundations. Ocean Eng 144: 203–210.
4. Chung JH, Chung HK, Song L (2011) Behavior of floating top-base foundation on soft soils by laboratory model tests. J Korean Geotech Soc 27(2): 5–15.
5. Dutt RN, Ingram WB (1988) Bearing capacity of jack-up footings in carbonate granular sediments. In: Proceedings of the First International Conference on Engineering for Calcareous Sediments, Perth, Australia, Vol. 1, Rotterdam, A.A. Balkema, pp. 291–296.
6. Gai GQ, Miao L, Chen HJ, Sun GH, Wu JQ, Xu YH (2013) Grain size and geochemistry of surface sediments in northwestern continental shelf of the South China Sea. Environ Earth Sci 70(1): 363–380.
7. Hagenaar J (1982) The use and interpretation of SPT results for the determination of axial bearing capacities of piles driven into carbonate soils and coral. In: Proceedings of the Second European Symposium on Penetration Testing, Amsterdam, Netherlands, pp. 51–55.
8. Hazzar L, Hussien MN, Karray M (2017) On the behaviour of pile groups under combined lateral and vertical loading. Ocean Eng 131: 174–185.
9. King R, Lodge M (1988) North west shelf development-the foundation engineering challenge. In: Proceedings of the First International Conference on Engineering for Calcareous Sediments, Perth, Australia, Vol. 2, Rotterdam, A.A. Balkema, pp. 333–341.
10. Lee JH, Tran NX, Kim SR (2019) Development and field application of GFRP suction pile. Ocean Eng 173: 308–318.
11. Lee MJ, Hong SJ, Kim R, Chae YH, Lee W (2012) Evaluation of cementation of Jeju coastal sediments using in situ tests. Bull Eng Geol Environ 71(3): 511–518.
12. Lin C, Han J, Bennett C, Parsons RL (2016) Analysis of laterally loaded piles in soft clay considering scour-hole dimensions. Ocean Eng 111: 461–470.
13. Liu CQ, Yang ZQ, Wang R (1995) The present condition and development in studies of mechanical properties of calcareous soils. Rock Soil Mech 16(4): 74–84.
14. Liu L, Liu HL, Xiao Y, Chu J, Xiao P, Wang Y (2018) Biocementation of calcareous sand using soluble calcium derived from calcareous sand. Bull Eng Geol Environ 77(4): 1781–1791.
15. Liu X, Li S, Sun LQ (2020) The study of dynamic properties of carbonate sand through a laboratory database. Bull Eng Geol Environ 79(7): 3843–3855.

16. Liu YC, Zuo GZ, Chen FQ (2007) Numerical research on stress distribution of geosynthetic reinforcement layer. Rock Soil Mech 28(5): 903–908.
17. Lu S, Tang HM, Zhang YQ, Gong WP, Wang LQ (2018) Effects of the particle-size distribution on the micro and macro behavior of soils: fractal dimension as an indicator of the spatial variability of a slip zone in a landslide. Bull Eng Geol Environ 77(2): 665–677.
18. Lv BQ, Wang GZ, Quan SQ (1987) Sedimentary characteristics and evolution arypattern of the sand clays in the xisha islands (in Chinese). Mar Geol Quat Geol 7(2): 59–69.
19. Lv YR, Li F, Liu YW, Fan PX, Wang MY (2017) Comparative study of coral sand and silica sand in creep under general stress states. Can Geotech J 54(11): 1601–1611.
20. Lv YR, Wang Y, Zuo DJ (2019) Effects of particle size on dynamic constitutive relation and energy absorption of calcareous sand. Powder Technol 356: 21–30.
21. Ma LL, Wang LZ, Guo Z, Jiang HY, Gao YY (2018) Time development of scour around pile groups in tidal currents. Ocean Eng 163: 400–418.
22. McClelland B (1988) Calcareous sediments: an engineering enigma. In: Proceedings of the First International Conference on Engineering for Calcareous Sediments, Perth, Australia, Vol. 2, Rotterdam, A.A. Balkema, pp. 777–784.
23. Mello JRC, Amaral C, Costa AM, Rosas M, Coelho PS, Porto E (1989) Closed-ended pipe piles: testing and piling in calcareous sand. In: Proceedings of the 21th Annual offshore technology conference, Houston, American, pp. 341–352.
24. Ministry of Housing and Urban-Rural Development of the People's Republic of China. Cold for design of building foundation (GB50007–2019) (in Chinese). Beijing: China Architecture & Building Press, 2019.
25. Ministry of Water Resources of the People's Republic of China. Standard for soil test method (SL 50123–2019) (in Chinese). Beijing: China Planning Press, 2019.
26. Ohno S, Ochiai H, Yasufuku N (1999) Estimation of pile settlement in calcareous sand. In: Proceedings of the Second International Conference on Engineering for Calcareous Sediments, Manama, Bahrain, Vol. 1, Rotterdam, A.A. Balkema, pp. 1–6.
27. Page AM, Grimstad G, Eiksund GR, Jostad HP (2018) A macro-element pile foundation model for integrated analyses of monopile-based offshore wind turbines. Ocean Eng 167: 23–35.
28. Rui SJ, Guo Z, Si TL, Li YJ (2020) Effect of particle shape on the liquefaction resistance of calcareous sands. Soil Dyn Earthq Eng 137: 106302.
29. Shaqour FM (2007) Cone penetration resistance of calcareous sand. Bull Eng Geol Environ 66(1): 59–70.
30. Shen Y, Zhu YH, Liu HL, Li A, Ge HY (2018) Macro-meso effects of gradation and particle morphology on the compressibility characteristics of calcareous sand. Bull Eng Geol Environ 77(3): 1047–1055.
31. Sui TT, Zhang C, Jeng DS, Guo YK, Zheng JH, Zhang W, Shi J (2019) Wave-induced seabed residual response and liquefaction around a mono-pile foundation with various embedded depth. Ocean Eng

173: 157–173.
32. Vesic AS (1973) Analysis of ultimate loads of shallow foundations. ASCE J Soil Mech Found Div 99(1): 45–73.
33. Wang H, Yang GQ, Xiong BL, Wu LH, Liu HB (2016) An experimental study of the structural behavior of reinforced soil retaining wall with concrete-block panel. Rock Soil Mech 37(2): 487–498.
34. Wang X, Zhu CQ, Wang XZ, Qin Y (2019) Study of dilatancy behaviors of calcareous soils in a triaxial test. Mar Georesour Geotechnol 2019; 37(9): 1057–1070.
35. Wang XM, Chen WL, Xue YL, Liu G (2018) The late quaternary carbonate sand deposits at the Xuande Atoll (in Chinese). Mar Geol Quat Geol 38(6): 37–45.
36. Wang XZ, Jiao YY, Wang R, Hu MJ, Meng QS, Tan FY (2011) Engineering characteristics of the calcareous sand in Nansha Islands, South China Sea. Eng Geol 120(1–4): 40–47.
37. Wang XZ, Wang X, Chen JW, Wang R, Hu MJ, Meng QS (2017c) Experimental study on permeability characteristics of calcareous soil. Bull Eng Geol Environ 77(4): 1753–1762.
38. Wang XZ, Wang X, Jin ZC, Zhu CQ, Wang R, Meng QS (2017a) Investigation of engineering characteristics of calcareous soils from fringing reef. Ocean Eng 134: 77–86.
39. Wang XZ, Wang X, Liu HF, Meng QS, Zhu CQ (2017b) Field test study of engineering behaviors of coral reef foundation. Rock Soil Mech 38(7): 2065–2079.
40. Wess JA, Chamberlin RS (1971) Khazzan Dubai No. 1: pile design and installation. ASCE J Soil Mech Found Div 97(10): 1415–1429.
41. Wiltise EA, Hulett JM, Murff JD, Brown JE, Hyden AM, Abbs AF (1988) Foundation design for external strut strengthening system for Bass Strait first generation platforms. In: Proceedings of the First International Conference on Engineering for Calcareous Sediments, Perth, Australia, Vol. 1, Rotterdam, A.A. Balkema, pp. 321–330.
42. Ye JH, Zhang ZH, Shan JP (2019) Statistics- based method for determination of drag coefficient for nonlinear porous flow in calcareous sand soil. Bull Eng Geol Environ 78(5): 3663–3670.
43. Yu KF, Song CJ, Zhao HT (1995) The characters of geomorphology and modern sediments of Yongxing Island, Xisha Islands (in Chinese). Trop Oceanol 14(2): 24–31.
44. Zhang L, Zhao MH, Shi CJ, Zhao H (2010) Bearing capacity of geocell reinforcement in embankment engineering. Geotext Geomembranes 28(5):475–482.
45. Zhang MS (1990) Quaternary reef stratigraphic division in hole Xiyong-1(in Chinese). Mar Geol Quat Geol 10(2): 57–64.
46. Hakami BA, Abu Seif ES (2019) Geotechnical aspects and associated problems of Al-Shuaiba Lagoon soil, Red Sea c, Saudi Arabia. Environ Earth Sci 78(5): 158.

Figures

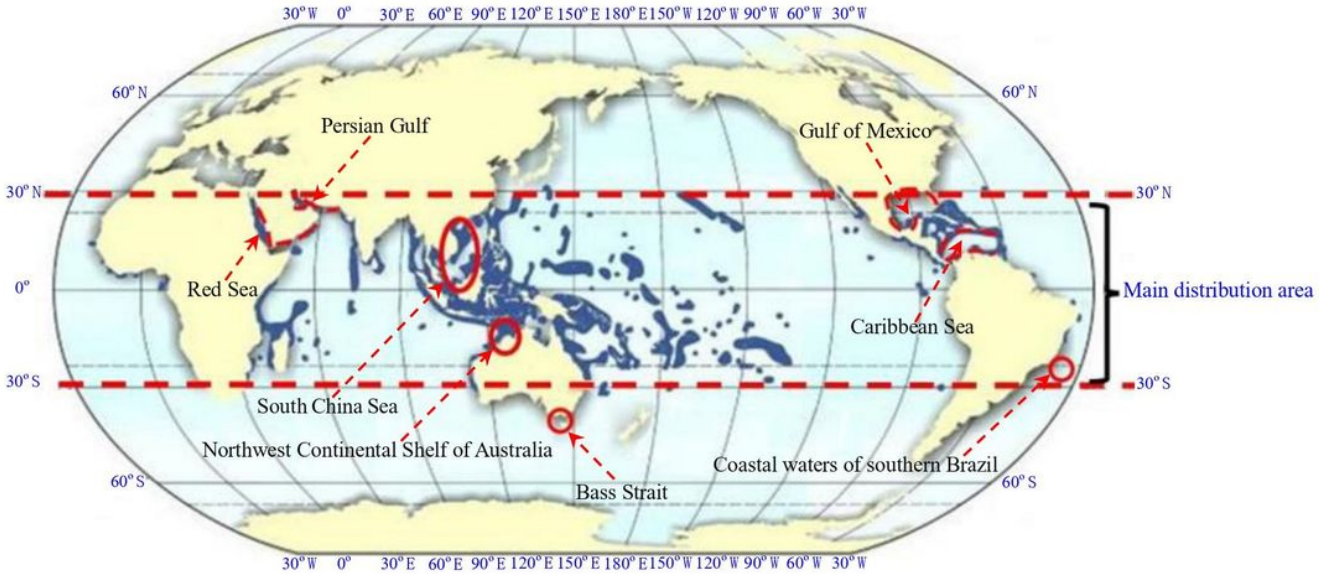

Figure 1

Main distribution area of calcareous sand. Note: The designations employed and the presentation of the material on this map do not imply the expression of any opinion whatsoever on the part of Research Square concerning the legal status of any country, territory, city or area or of its authorities, or concerning the delimitation of its frontiers or boundaries. This map has been provided by the authors.

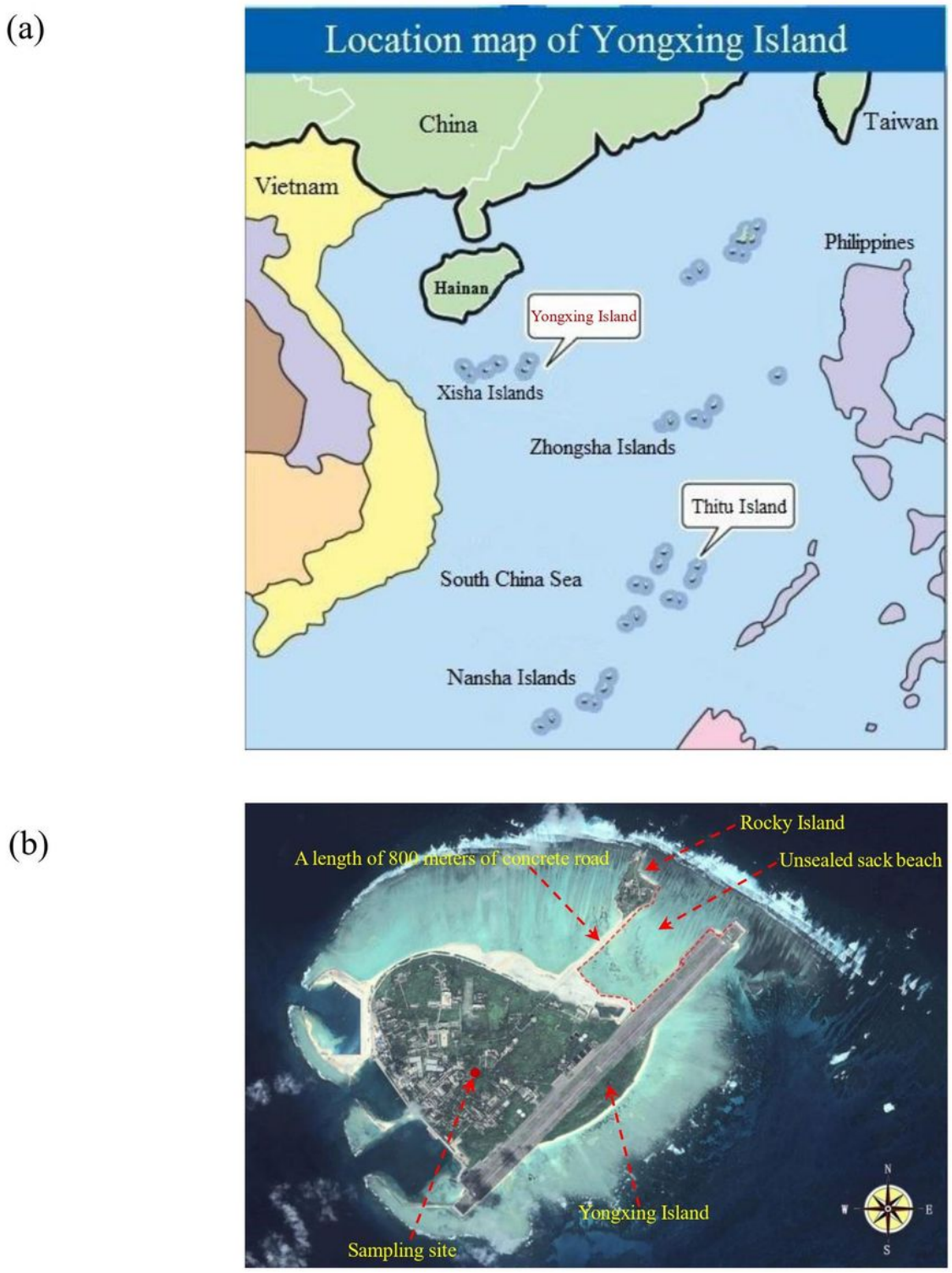

Figure 2

Study area (a: location of Yongxing Island; b: Yongxing Island after expansion). Note: The designations employed and the presentation of the material on this map do not imply the expression of any opinion whatsoever on the part of Research Square concerning the legal status of any country, territory, city or area or of its authorities, or concerning the delimitation of its frontiers or boundaries. This map has been provided by the authors.

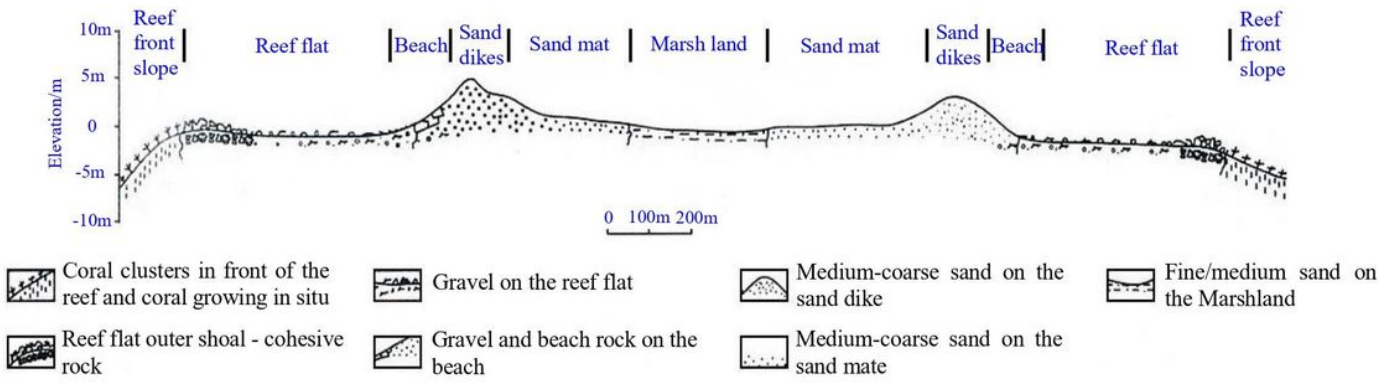

Figure 3

Landform distribution profile of Yongxing Island (Yu et al. 1995).

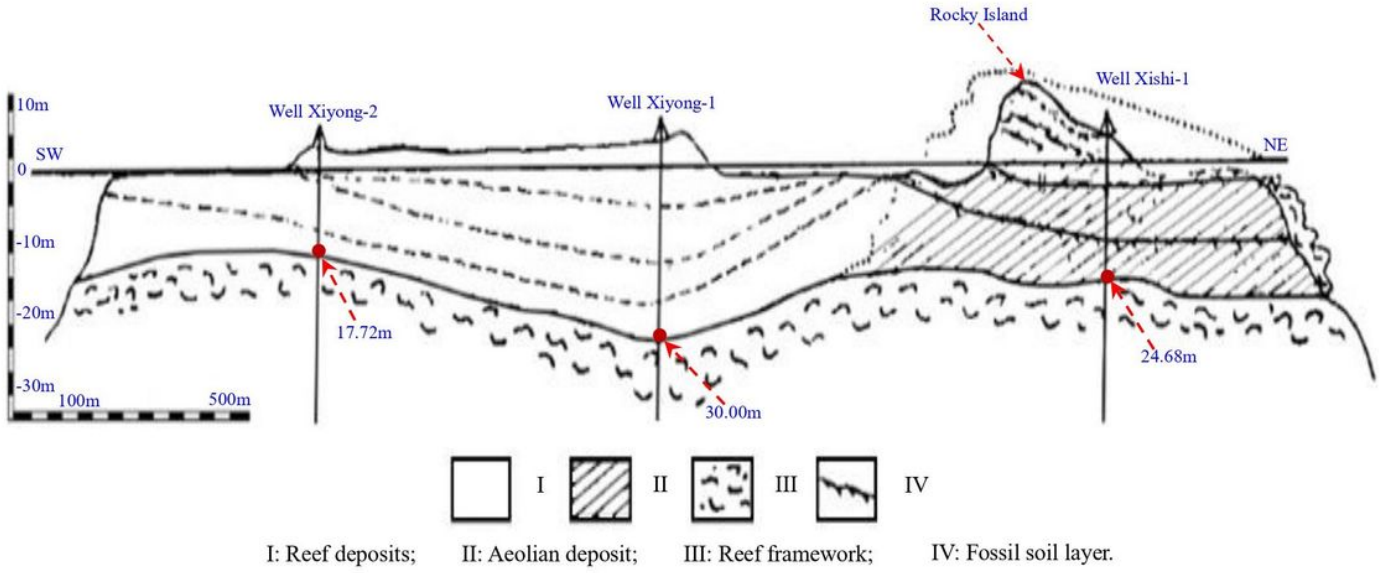

Figure 4

Drilling sections for Yongxing Island and Rocky Island (Zhang 1990).

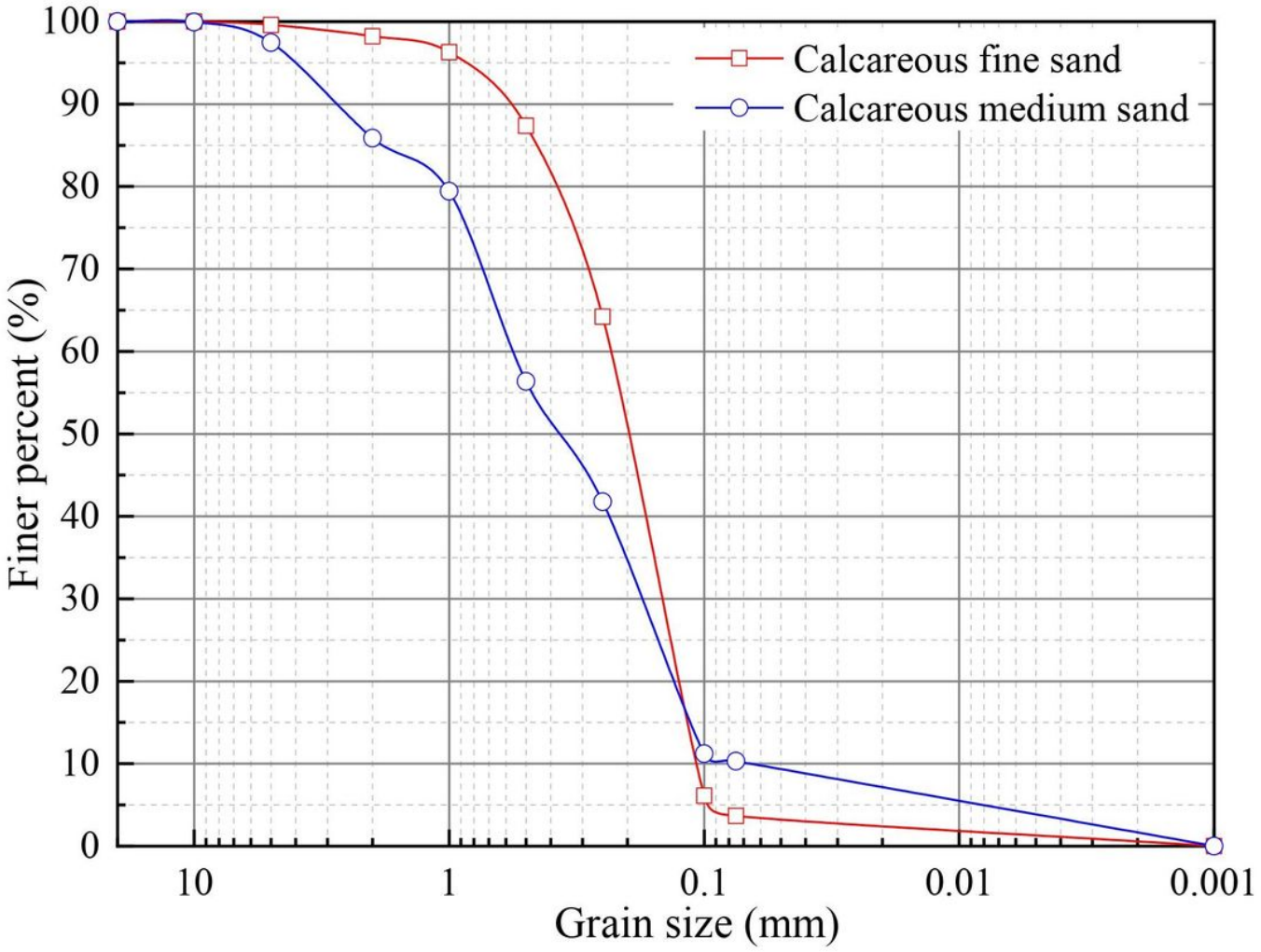

Figure 5

Grain size distribution curve of the soil samples.

Figure 6

Laboratory plate loading test device.

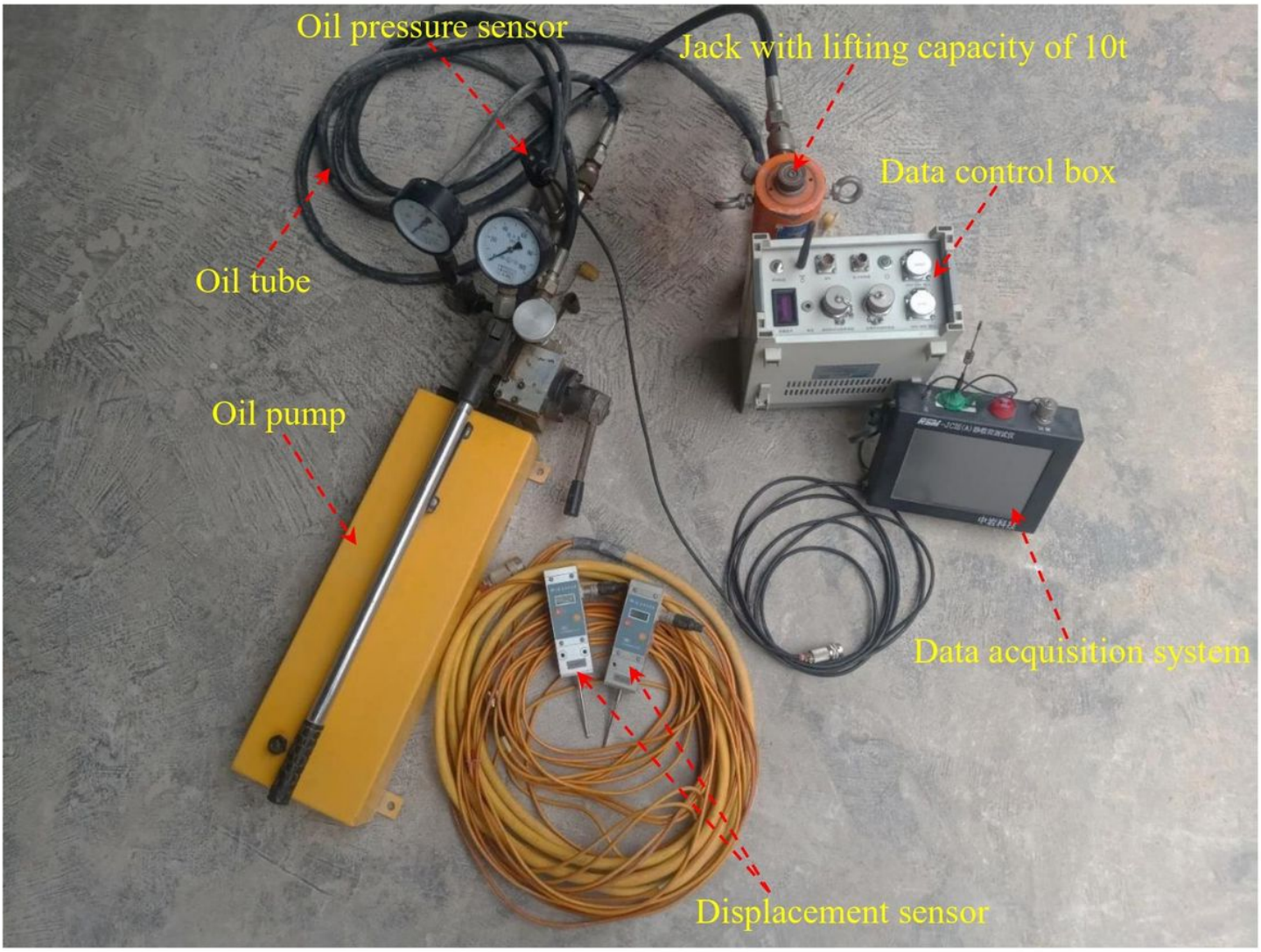

Figure 7

Static loading system.

(a)

(b)

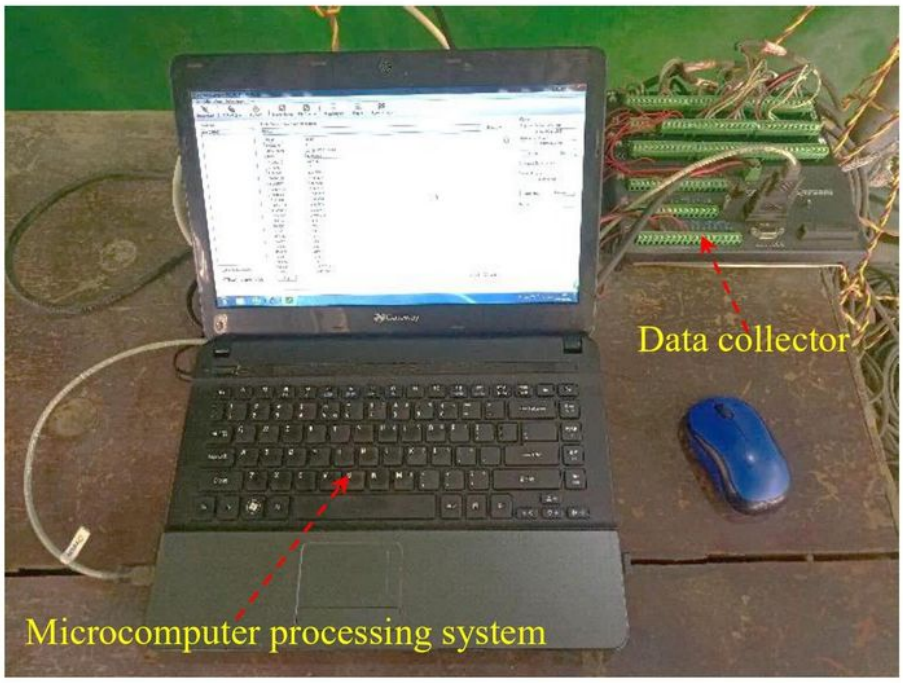

Figure 8

Lateral stress measurement system (a: soil pressure gauge; b: data collector and microcomputer processing system).

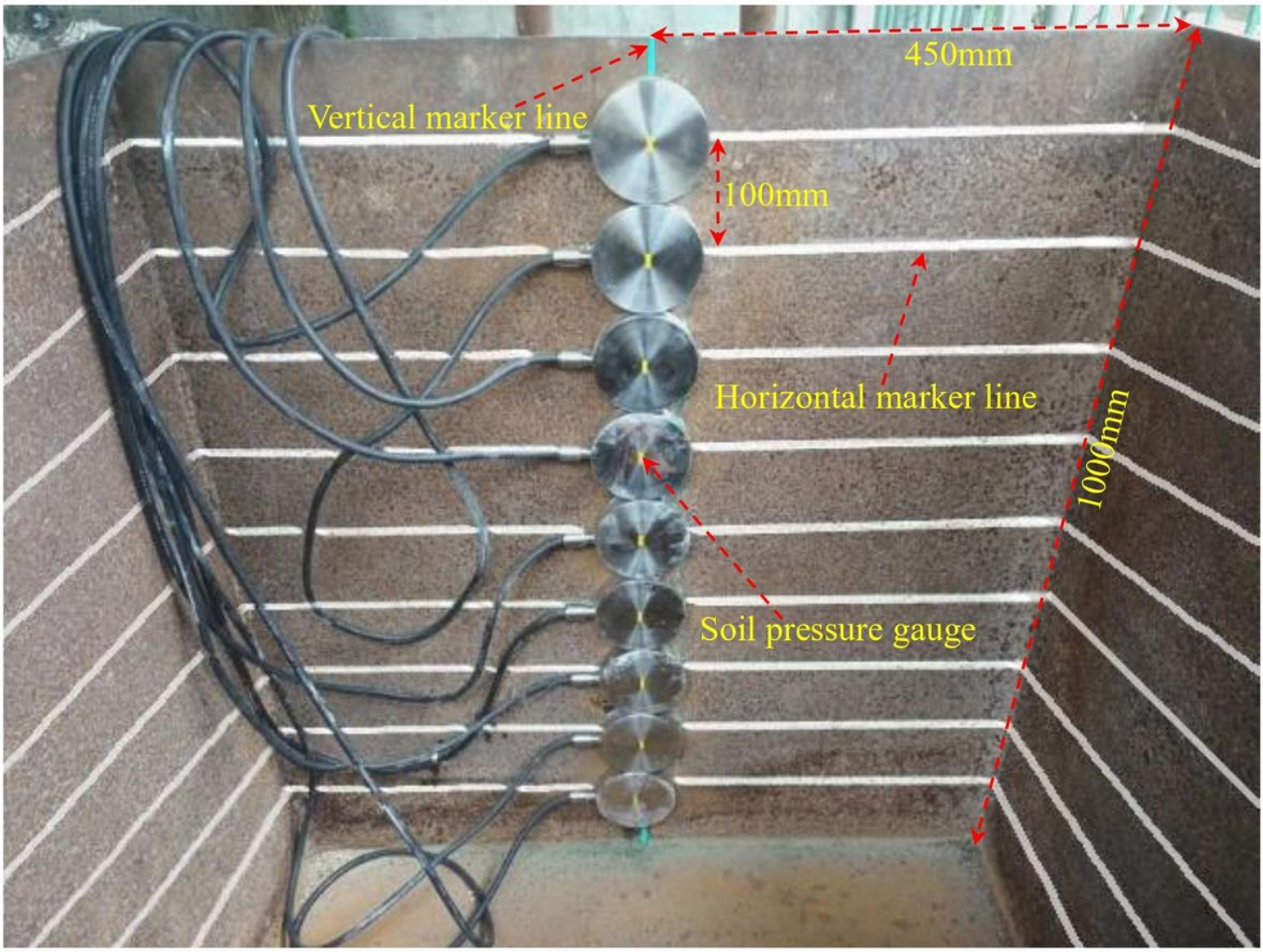

Figure 9

Location of the soil pressure gauges.

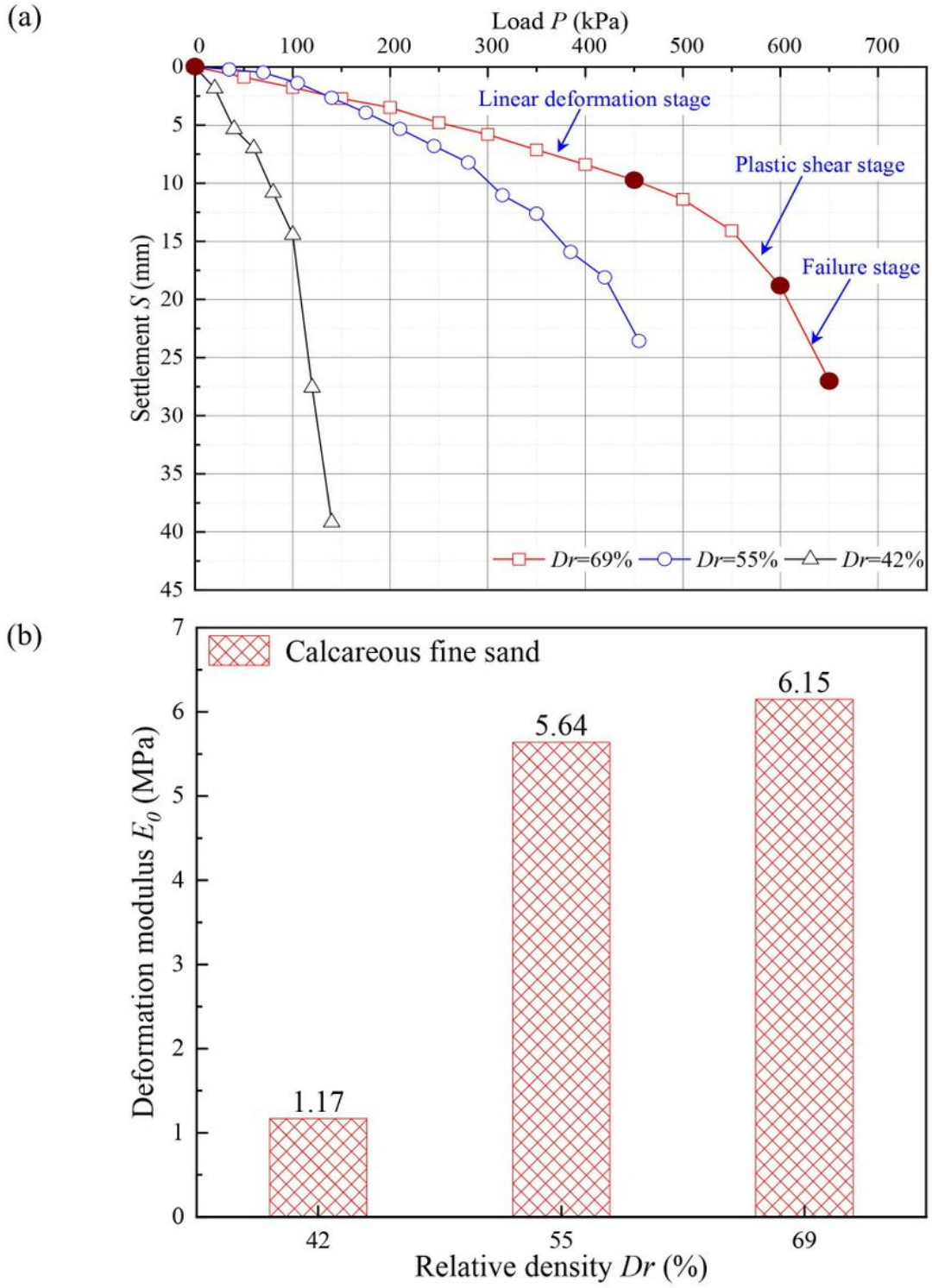

Figure 10

Results of the plate loading tests on calcareous fine sand foundations with different relative densities (a: P-S curves; b: histogram of deformation modulus versus relative density).

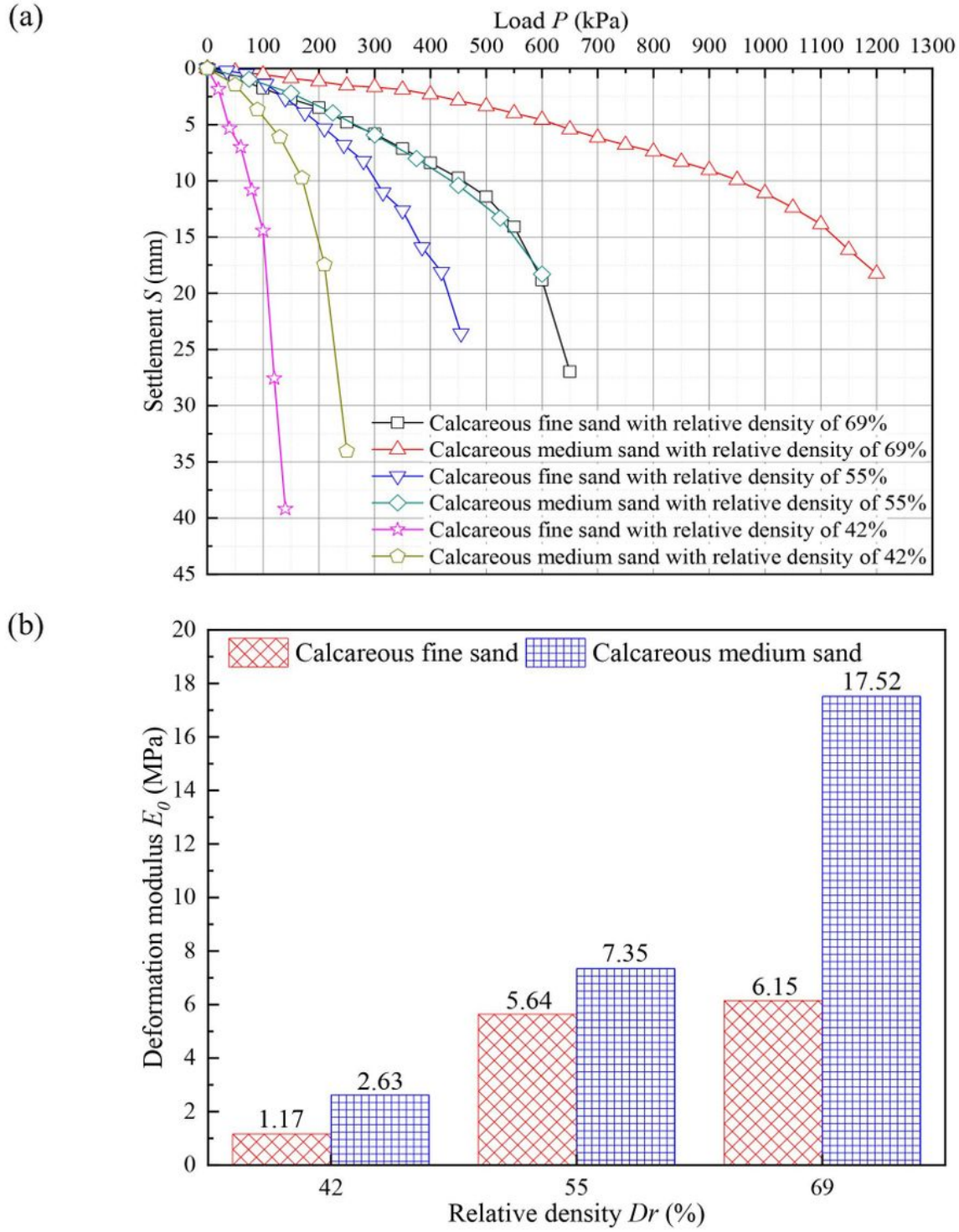

Figure 11

Results of the plate loading tests on calcareous sand foundations of different particle gradations (a: P-S curves; b: histogram of deformation modulus versus relative density).

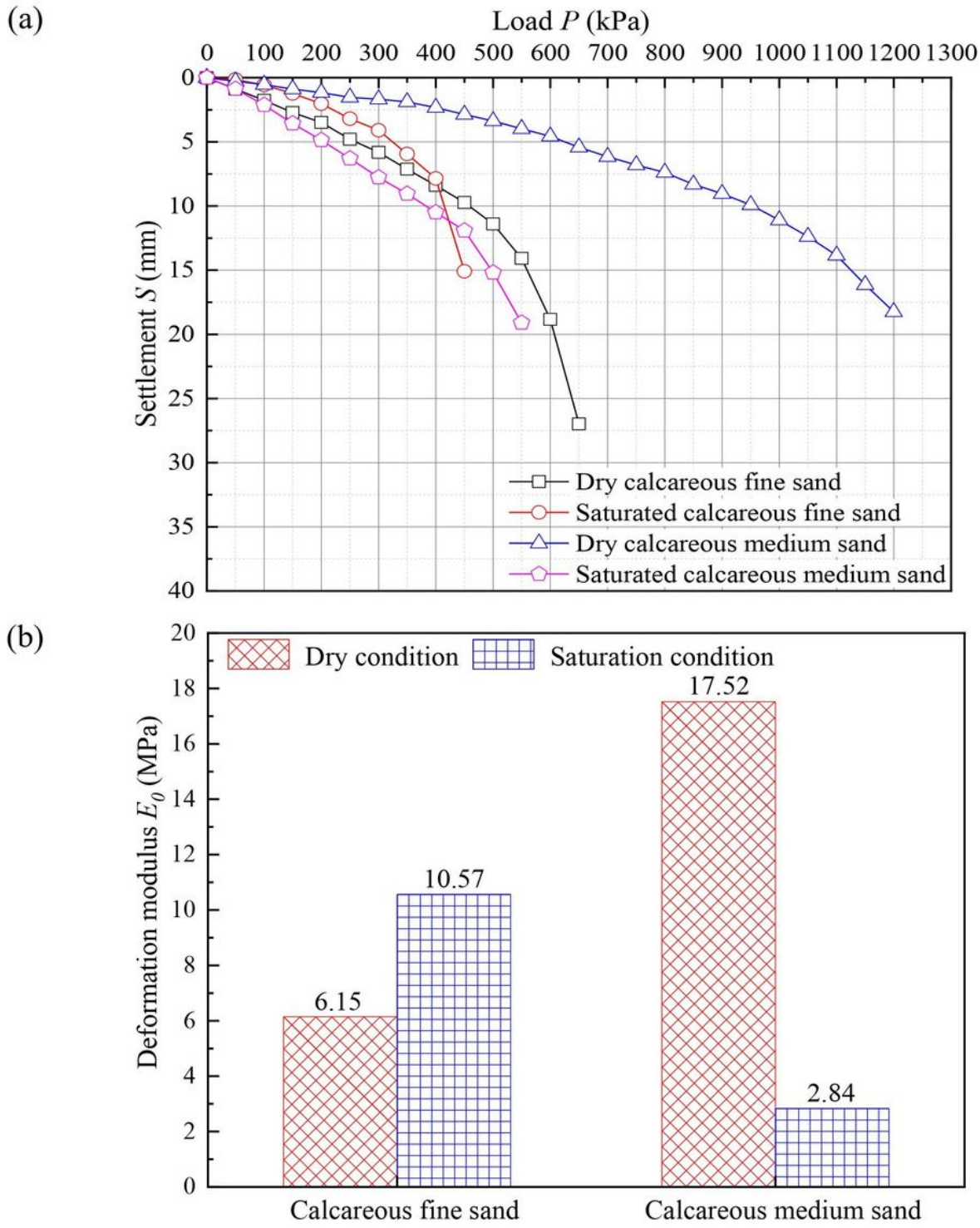

Figure 12

Results of the plate loading tests on calcareous sand foundations under different mositure conditions (a: P-S curves; b: histogram of deformation modulus versus relative density).

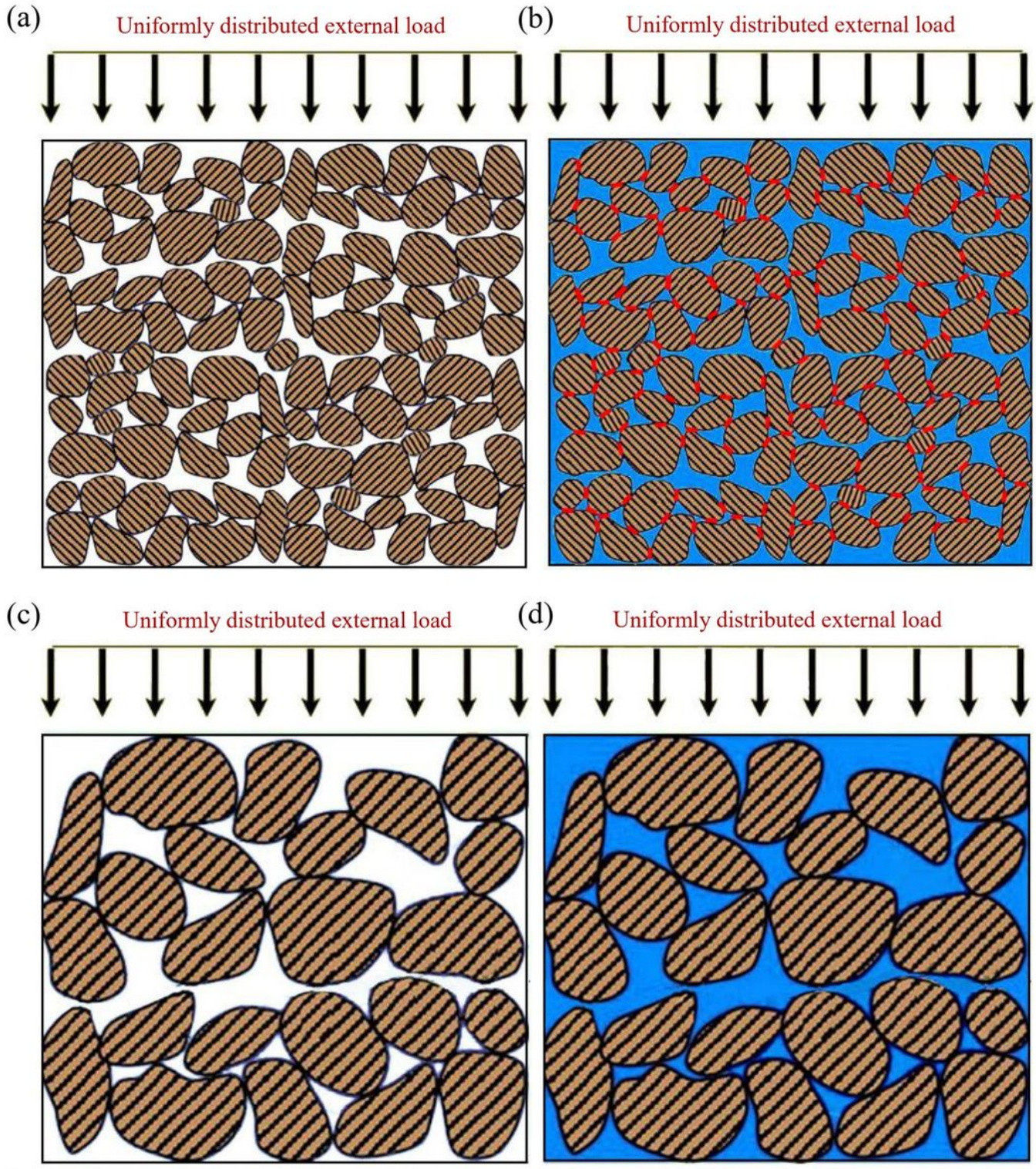

Figure 13

Schematic structural diagram of calcareous sands with different physical states (a: dry calcareous fine sand; b: saturated calcareous fine sand; c: dry calcareous medium sand; d: saturated calcareous medium sand).

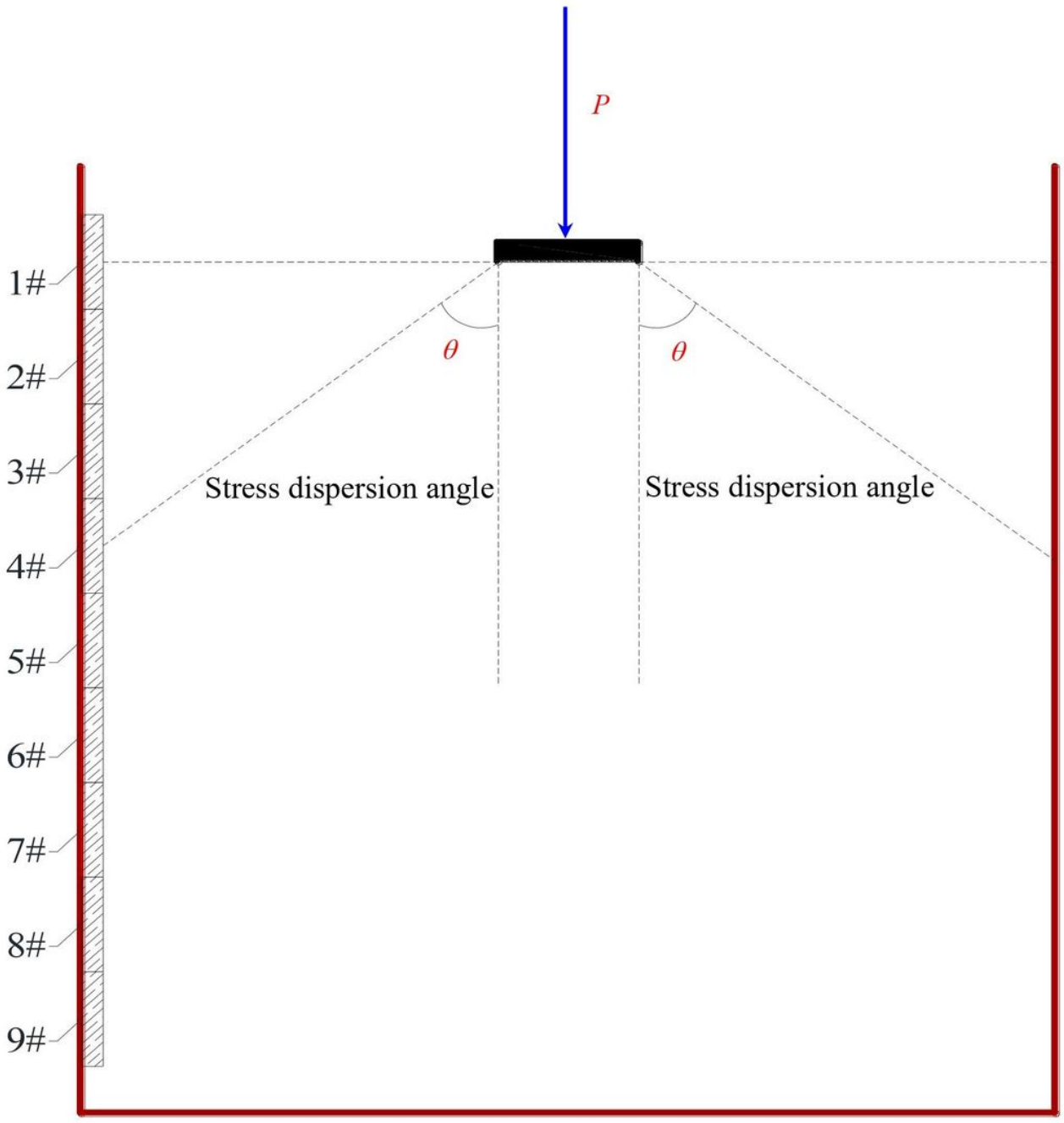

Figure 14

Schematic diagram showing the positions of the soil pressure gauges and the stress dispersion angle.

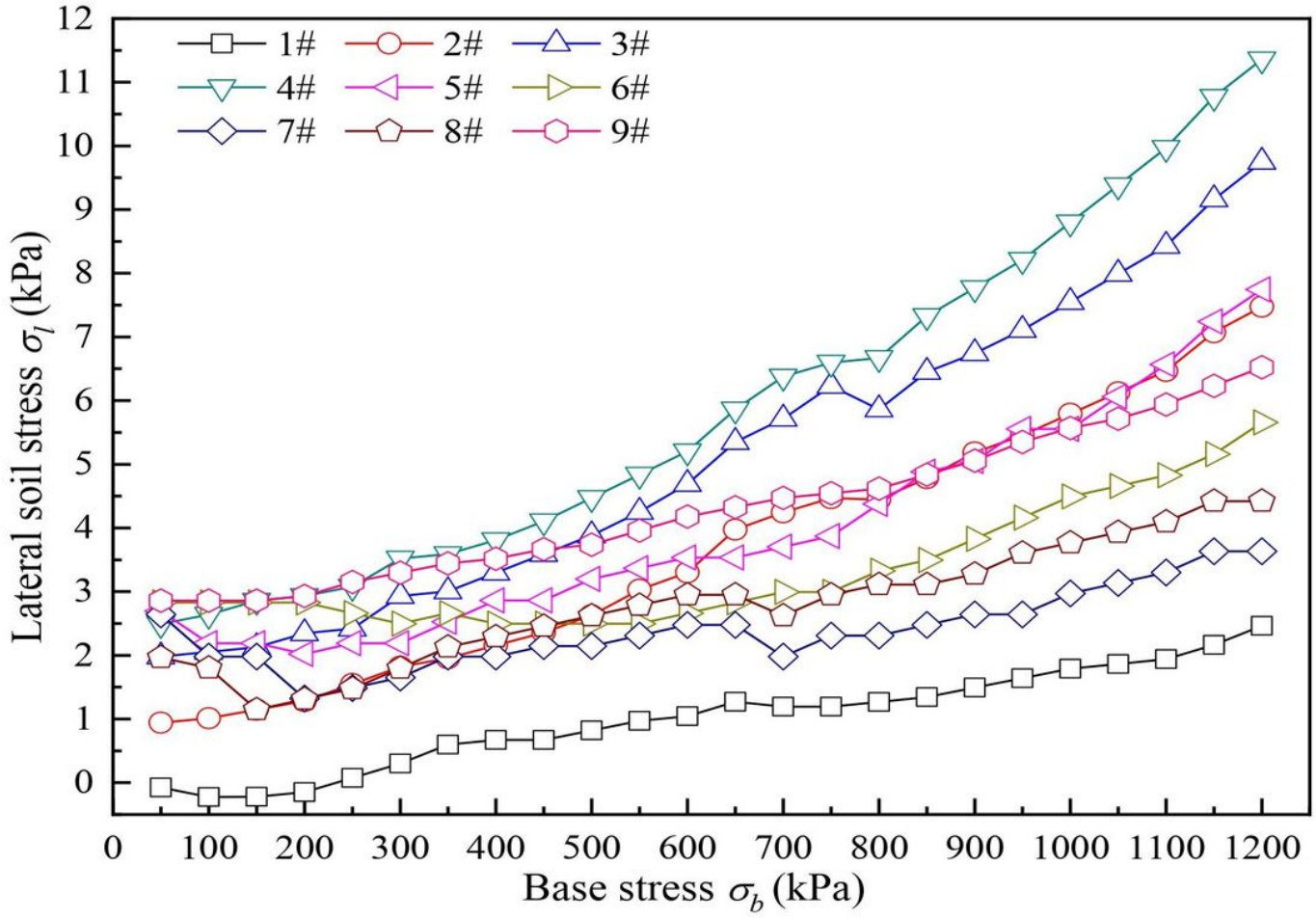

Figure 15

Plot of lateral soil stress versus base stress for different depths.

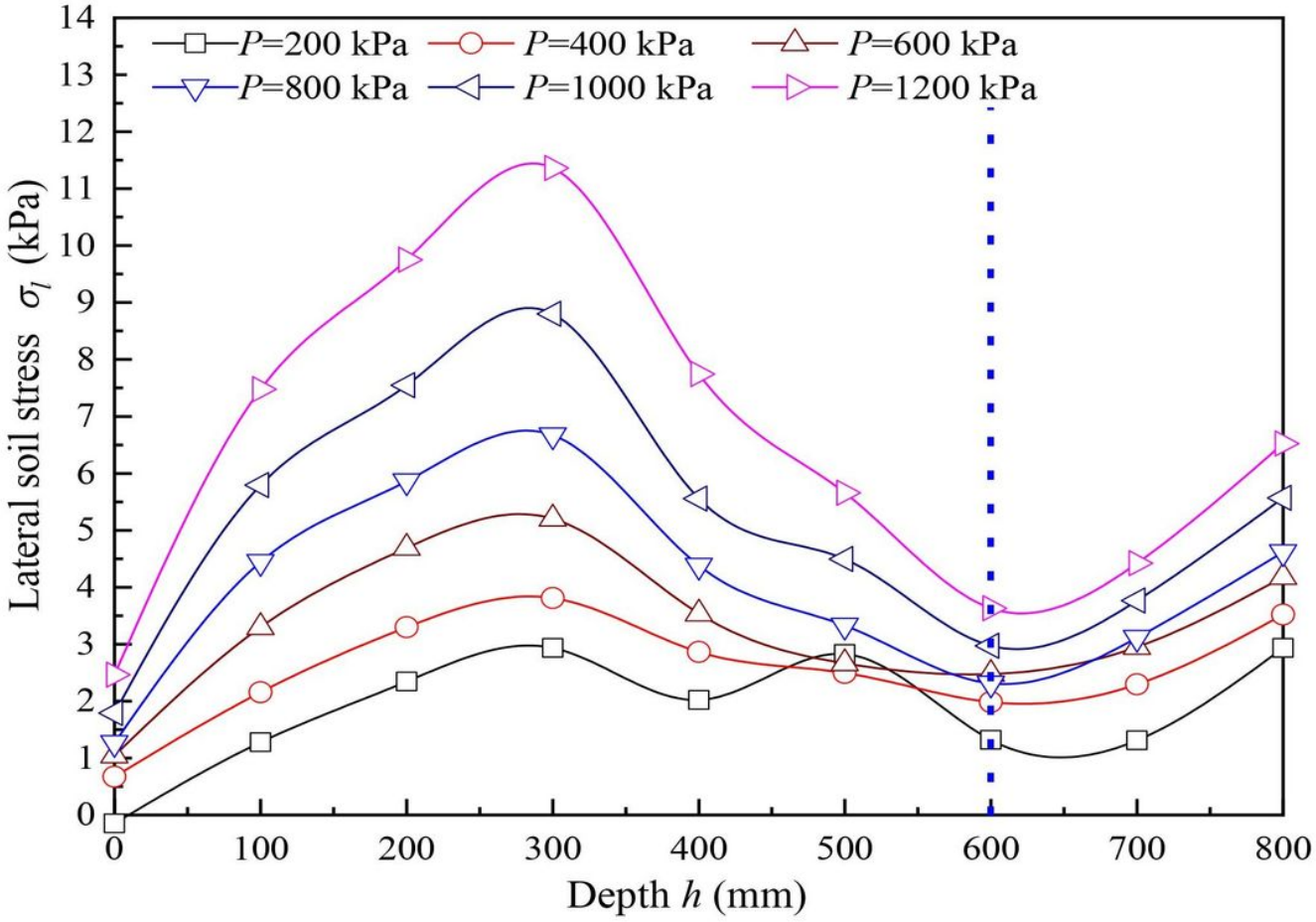

Figure 16

Plot of lateral soil stress versus depth under different base stresses.